Static and dynamic magnetic properties of a localized moment: NMR of ^{59}Co in dilute *Mo*Co and *W*Co alloys*

A. Narath
Sandia Laboratories, Albuquerque, New Mexico 87115
(Received 15 December 1975)

Because of unusually small cobalt hyperfine fields it has been possible to study the static and dynamic properties of the Kondo alloys *Mo*Co and *W*Co in considerable detail by means of impurity NMR techniques. Measurements are reported for the temperature range 1–~500 K in magnetic fields to 130 kOe. From the Curie-Weiss behavior of the weak-field resonance shifts Kondo temperatures $\Theta_K = 45(3)$ K and 1.8(2) K are obtained for the two alloys, respectively. The corresponding hyperfine fields are $H_{hf} = -26$ and -1.5 kOe/μ_B. The g values are $g = 1.3$ and 1.4. A consistent interpretation of our data is achieved by means of an ionic model with a Γ_2 orbital singlet ground state arising from the Co^{2+} $3d^7$ (^4F) term in the presence of crystal-field, spin-orbit, and local-moment–conduction-electron exchange perturbations. The small hyperfine fields are attributed to spin-orbit induced orbital contributions, and the negative g shifts to the exchange coupling. Measurements of the ^{59}Co relaxation rates T_2^{-1} in *W*Co over a wide range of temperatures and magnetic field strengths give evidence for competing local-moment fluctuation and direct conduction-electron mechanisms. The former dominates at temperatures below ~50 K; in applied fields above ~100 kOe this relaxation process can be explained satisfactorily by means of standard perturbation theory. With decreasing field strength Kondo anomalies become increasingly important and the nuclear relaxation rate appears to saturate as predicted by simple scaling arguments.

I INTRODUCTION

In contrast to the more usual nonmagnetic behavior of isolated cobalt impurities in metallic hosts such as aluminum and the noble metals, dilute *Mo*Co and *W*Co alloys exhibit well-defined local-moment properties. At high temperatures their susceptibilities approximate Curie laws with effective moments near[1-3] $3\mu_B$; at low temperatures typical Kondo anomalies are observed in the magnetic and transport properties.[4,5] Among the interesting characteristics of these alloys are suprisingly small cobalt hyperfine fields[6] (10^3–10^4 Oe/μ_B) which are responsible for unusually slow local-moment-induced nuclear relaxation rates. As a consequence, the ^{59}Co nuclear magnetic resonances (NMR) are experimentally accessible over a wide range of temperatures and applied field strengths, making it possible to probe the local magnetic properties in considerable detail.

The work reported here is concerned with a detailed ^{59}Co NMR study of the static as well as dynamic magnetic properties of *Mo*Co and *W*Co. It is an extension of an earlier NMR investigation (hereafter referred to as I)[7] which explored the possibility of nonperturbative conduction-electron spin-correlation contributions to the field-induced magnetization of dilute magnetic alloys below the Kondo temperature (Θ_K). Results of ^{59}Co, ^{95,97}Mo, and ^{183}W NMR measurements reported in I provided no evidence for such anomalous behavior. Instead, the magnetic properties of *Mo*Co and *W*Co were shown to be strikingly similar to those of *Au*V,[8,9] an alloy whose high Kondo temperature ($\Theta_K \sim 300$ K)[10] places it between the magnetic (Kondo) and nonmagnetic (spin-fluctuation) regimes of the magnetic-impurity problem. The absence of anomalous spin-polarization effects in *Au*V had been demonstrated previously.[8]

The principal objective of the present study is to clarify a number of points which were not treated adequately in I, and thus to develop a more detailed understanding of the magnetism of cobalt impurities in these alloys. Many of the earlier uncertainties are a consequence of the low solubility of cobalt in molybdenum and tungsten[11,12] together with its high vapor pressure at the solvent melting temperatures, which make the preparation of homogeneous, single-phase alloys extremely difficult. Among the unresolved questions is the origin of a second (nonmagnetic) ^{59}Co resonance which was observed in all samples of *Mo*Co as well as *W*Co and whose intensity increased very rapidly with increasing cobalt concentration, suggesting the formation of nonmagnetic cobalt clusters. More importantly, at temperatures below ~30 K the ^{59}Co resonance shift in *Mo*Co was found to be concentration dependent and to deviate strongly from the expected $(T+\Theta_K)^{-1}$ dependence, assuming $\Theta_K = 24$ K as given by the magnetic-susceptibility measurements of Booth *et al.*[1] Although more recent experiments suggest a higher Kondo temperature ($\Theta_K \approx 60$ K,[2,3]

and[5] 46 K) apparently in better agreement with the NMR results, some uncertainty remains because of the unknown influence of magnetic and/or nonmagnetic cobalt clusters on the measured bulk susceptibilities. The ^{59}Co and ^{183}W NMR shifts in *W*Co were in reasonable agreement with published susceptibility data ($\Theta_K = 11$ K)[1]; however, the poor resolution of magnetic and nonmagnetic resonances in the available alloy samples made such a conclusion tentative. The possibility of magnetic-saturation effects on the observed low-temperature resonance shifts and relaxation rates in *W*Co was also not explored.

Our experimental techniques are briefly summarized in Sec. II. The experimental results for *Mo*Co and *W*Co are presented in Secs. III A and III B, respectively. An analysis of the data is carried out in Sec. IV and our conclusions are summarized briefly in Sec. V.

II. EXPERIMENTAL TECHNIQUES

A. Instrumental details

The NMR experiments were carried out with pulsed (coherent spin-echo) or cw spectrometers, as appropriate, and generally followed the techniques described in I. A high-power frequency multiplier[13] was added for the high-field experiments in order to extend the range of our earlier 2–40-MHz spin-echo spectrometer. Magnetic fields, to 130 kOe, were provided by a Nb_3Sn superconducting solenoid (Intermagnetics Corp.). Field regulation and control were accomplished by means of a multiturn copper magnetoresistance probe wound on the sample Dewar inside the solenoid bore. Field-strength calibrations were based on the ^{27}Al NMR in aluminum metal [$\nu(\mathrm{Al})^{27}/H = 1.1112$ kHz/Oe at 4 K]. At the higher frequencies and low temperatures rf heating became a serious problem and special precautions (e.g., reduced pulse repetition rates, dilution of sample powders with nonmetallic material, and direct contact of the sample particles with the cryogenic fluid) were necessary to assure reliable data.

Signal averaging was used extensively because of poor signal/noise ratios resulting from the low cobalt concentrations and severe line broadening. As discussed in I, only the $+\frac{1}{2} \rightleftharpoons -\frac{1}{2}$ transition is observed in the ^{59}Co experiments (presumably because of first-order quadrupole effects associated with random sample strains), thus, further reducing the signal intensity. Resonance-shift as well as relaxation (spin-echo phase-memory time T_2) measurements utilized repetitive field sweeps through resonance. For spin-echo experiments the signal was detected with a Princeton Applied Research cw-1 "boxcar" integrator. The outputs of both cw and pulsed spectrometers were accumulated in a Nicolet 1074 multichannel analyzer whose sweep was synchronized with the field sweep. Errors due to drifts in spectrometer sensitivity were minimized in T_2 measurements requiring long averaging times by alternating the time separation of the two sampling pulses in successive sweeps between a particular value (τ) and a very small ($\tau_0 = 0$) reference value. These sweeps were stored in separate memory blocks; the ratio of the two resonance intensities yielded a direct measure of the fractional phase-memory decay during the time interval $\tau - \tau_0$. Sweep durations were typically 10 min and approximately 200 sweeps were required for adequate signal intensities at the highest temperatures. A complete decay curve was established by repeating the experiment several times using different τ values. The resulting curves were always exponential functions of time within our experimental uncertainties. As already discussed in I, it was not possible to determine spin-lattice relaxation times (T_1) directly by means of pulse-saturation techniques because of excessive quadrupole broadening.

Resonance shifts were determined at constant frequencies from the measured field strengths at maximum signal intensity using the ^{59}Co reference frequency/field ratio[14]

$$\nu_{\mathrm{ref}}(^{59}\mathrm{Co})/H = 1.005 \text{ kHz/Oe} . \tag{2.1}$$

This ratio differs from the value 1.010 kHz/Oe used in I. The magnitudes of the present shift values (in percent) consequently exceed those based on the older reference by 0.5. Our conclusions are insensitive to this change.

B. Alloy preparation

The alloys studied in I were prepared by powder metallurgical techniques[1] using mixed powders of the elemental metals. Attempts to improve alloy homogeneity, as judged by the ^{59}Co NMR linewidth and the ratio of magnetic to nonmagnetic resonance intensities, focused on several different preparation methods. These fall into four general categories: (i) arc melting of the elemental metals in an inert atmosphere, (ii) sintering of the powdered metals after high-pressure densification, (iii) coprecipitation from acid solution followed by hydrogen reduction, and (iv) mixing of the molten oxides followed by rapid quenching and hydrogen reduction.

The arc-melting technique yielded uniformly poor results. In every case complex NMR spectra were observed which gave evidence for multiple nonmagnetic phases. Arc-melted *Mo*Co alloys used in the susceptibility experiments of Claus[2] yielded similar NMR results. Whether this be-

havior is characteristic of arc-melted *Mo*Co and *W*Co alloys or is a consequence of cold-work induced changes during alloy comminution is not known. In this connection it should be noted that the other preparation methods listed above yield alloys that require little if any crushing for the desired 300–400-mesh powders, thus minimizing any cold-working problems.

The powder-metallurgical sintering technique proved to be superior for *Mo*Co alloys. Compared to the alloys used in I, improved solute dispersion, particularly at low concentrations, was achieved by mixing the molybdenum powder (325 mesh, 99.999% purity) with an aqueous solution of $CoCl_2$ instead of powdered cobalt metal. [The $CoCl_2$ solution was prepared by dissolving cobalt metal (99.999% purity) in aqueous HCl.] After drying, the $CoCl_2$-coated molybdenum powders were reduced in H_2 at 800 °C for 4 h. They were subsequently pressed into $\frac{1}{2}$-in. diameter discs in a 40 000-lb press and homogenized in a H_2 atmosphere for 72 h at 1350 °C followed by 72 h at 1500 °C. The ^{57}Fe Mössbauer effect (ME) was found to be an effective diagnostic tool, particularly when used in combination with the ^{59}Co NMR. This is illustrated in Fig. 1 which compares spectra of two different 0.1-at% *Mo*Co alloys with those of the intermetallic compound Mo_6Co_7. (The

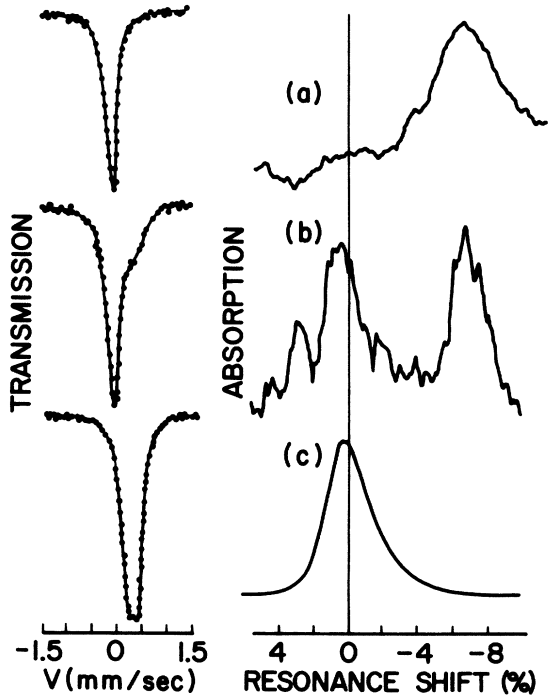

FIG. 1. Comparison of cobolt ME and NMR spectra for (a), (b) 0.1-at.% *Mo*Co alloys as described in text, and (c) Mo_6Co_7.

compound was prepared by thermal decomposition of $CoCO_3$ in a stoichiometric mixture of MoO_3 and $CoCO_3$ at 825 °C, followed by H_2 reduction at 1000 °C for 48 h.) The samples contained a small amount of ^{57}Co activity and were used as ME sources together with a single-line potassium ferrocyanide trihydrate absorber. The ME and NMR were studied in identical (i.e., radioactive) alloy samples. A separate Mo_6Co_7 sample, not containing the ^{57}Co activity, was prepared for the NMR experiment. Figure 1(a) shows results for a *Mo*Co alloy prepared as described above. The ME gives a single-line spectrum with a shift $\nu_1 = -0.095$ mm/sec and a width $\Gamma_1 = 0.26$ mm/sec. The NMR exhibits the cobalt local-moment resonance shifted to high fields (i.e., negative shift) and a very weak unshifted signal. The latter is the nonmagnetic cobalt resonance discussed in I. Alloys homogenized at lower temperatures typically contained a higher faction of nonmagnetic cobalt solute. This is illustrated in Fig. 1(b) for a sintered alloy which had been heat treated for 56 h at 600 °C. A definite shoulder is observed in the ME spectrum corresponding to $\nu_2 = +0.32$ mm/sec, $\Gamma_2 = 0.45$ mm/sec and an intensity which is 16% of the total. [The main peak yields $\nu_1 = -0.094$ mm/sec and $\Gamma_1 = 0.26$ mm/sec, in close agreement with Fig. 1(a).] The second peak in the ME spectrum evidently corresponds to the unshifted ^{59}Co NMR signal. Comparison of the alloy spectra with Fig. 1(c) suggests that the nonmagnetic component is caused by the formation of the intermetallic compound Mo_6Co_7. The Mo_6Co_7 ME spectrum consists of a doublet (presumably of quadrupolar origin) with $\nu_2 = 0.32$ mm/sec and $\Delta\nu = 0.02$ mm/sec. As indicated in Figs. 1(a) and 1(b), the NMR appears to be more sensitive to the nonmagnetic component than is the ME. Since the particle size exceeds the rf skin depth at the 40-MHz frequency used in these experiments, the apparent disparity is most likely due to concentration gradients in our samples. The probability of compound formation is highest near the surface of the powder particles because of the initially high cobalt concentration in this region. The fact that particles obtained by crushing the sintered alloy specimens are essentially identical to the particles in the starting material would thus account for our results. This interpretation is strengthened by the observation that the ratio of nonmagnetic to magnetic NMR signal intensities increases with increasing frequency (i.e., with decreasing skin depth).

The best *W*Co alloys were prepared by means of the coprecipitation technique. Tungsten metal (99.999% purity) was dissolved in a 1:1 mixture of concentrated HF and HNO_3 to which the desired

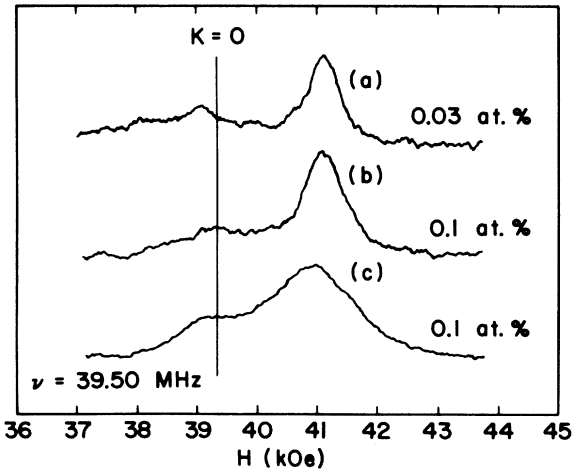

FIG. 2. Comparison of ^{59}Co NMR spectra in *W*Co. The alloys (a) and (b) were prepared by the coprecipitation technique; alloy (c) was prepared by the standard sintering technique.

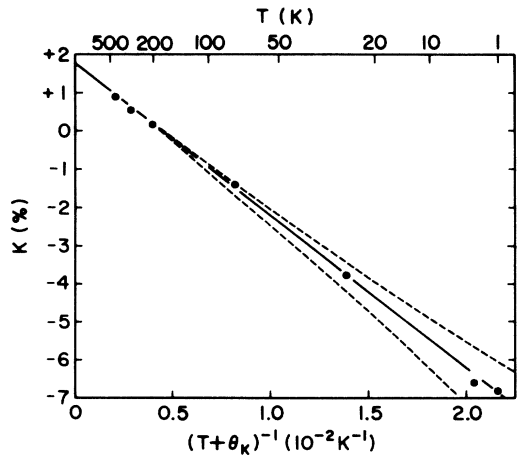

FIG. 3. Temperature dependence of ^{59}Co resonance shifts in 0.1 at.% *Mo*Co. The solid line corresponds to $\Theta_K = 50$ K, the upper and lower dashed lines to $\Theta_K = 45$ and 55 K, respectively.

quantity of aqueous $CoCl_2$ was added. The acid solvent was evaporated and the resulting bright-yellow material ground into a fine powder (325 mesh). Reduction was accomplished in a stream of H_2 using a quartz-tube furnace at 1000 °C. After the first 4 h the partially reduced grey-black powder was reground and the reduction continued for another 20 h. The improvement in alloy homogeneity, compared to the sintered alloys studied in I, is demonstrated by the ^{59}Co NMR spectra in Fig. 2. The intensity of the nonmagnetic-site resonance (which presumably is associated with a W_6Co_7 second phase) as well as the width of the magnetic-site resonance are seen to be significantly reduced.

III. EXPERIMENTAL RESULTS

A. *Mo*Co

The temperature dependence of the ^{59}Co resonance shift, $K \equiv \Delta H/H$, was measured in the range 1–420 K. The results for a 0.1-at.% alloy are plotted in Fig. 3 as a function of $(T+\Theta_K)^{-1}$, where $\Theta_K = 45 \pm 3$ K was chosen on the basis of a best fit of the data to the form

$$K = K_0 + K(T) . \tag{3.1}$$

Here $K_0 = 1.8 \pm 0.1\%$ is a temperature-independent term which can be attributed to the combined effects of local-moment Van Vleck and conduction-electron susceptibilities. The temperature-dependent term $K(T)$ is proportional to $(T+\Theta_K)^{-1}$. The predicted behaviors for $\Theta_K = 40$ and 50 K, as indicated by the dashed lines in Fig. 3, are seen to fall outside the experimental uncertainty. The present data are in excellent agreement with results discussed in I provided that account is taken of the different ^{59}Co reference ratios. (The earlier work only covered temperatures to 300 K and was restricted to higher cobalt concentrations in the

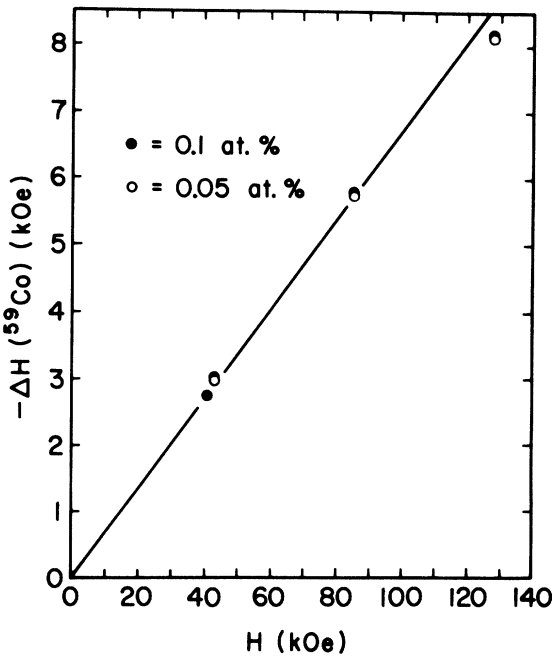

FIG. 4. Comparison of ^{59}Co resonance shifts in *Mo*Co for two solute concentrations at 1.2 K.

high-temperature region.) The concentration dependence of the low-temperature shifts, reported in I, is only observed at concentrations above 0.1 at.%. This can be seen in Fig. 4 which shows that the 0.1- and 0.05-at.% data are indistinguishable at 1.2 K. The shifts plotted in Fig. 4 are linear in field strength to ~100 kOe. The absence of significant saturation effects below 100 kOe is consistent with the high Kondo temperature deduced from the K vs T measurements.

B. *W*Co

The ^{59}Co resonance shifts were determined for a 0.1-at.% alloy in the range 1–500 K. As in the case of *Mo*Co the observed temperature dependence can be described by (3.1). The results shown in Fig. 5 yield $K_0 = 1.6(\pm 0.1)\%$ and $\Theta_K = 1.8(\pm 0.2)$ K. The Curie-Weiss behavior of the resonance shifts is exhibited more clearly in Fig. 6. The Kondo temperature is significantly lower than previously believed.[1] Our earlier low-temperature results, which were obtained in external fields near 40 kOe, consequently fall outside the linear magnetization regime for *W*Co. The shifts plotted in Figs. 5 and 6 were measured in sufficiently weak fields (10 kOe at liquid-helium temperatures) to represent the initial slope $\Delta H/H$.

It was possible to study the saturation behavior of the local-moment magnetization in some detail because of the large magnitudes of $g\mu_B H/[k_B(T+\Theta_K)]$ which were attainable in our experiments. The resonance-shift data are plotted in Fig. 7 for several temperatures as a function of applied field strength. These experiments were again performed on 0.1-at.% alloys. Measurements on a 0.03-at.% alloy at 40 and 120 kOe verified the absence of a detectable concentration dependence in the resonance shifts. The sign reversal in the slope $\Delta H/H$ is a direct consequence of magnetic saturation of the cobalt local moments. It is apparent that the positive slope at high fields has the same origin as the temperature-independent term (K_0) which was identified in Fig. 5. Any contribution to K which is independent of temperature in the range $0 < T \lesssim T_{max}$ is, of course, also expected to be independent of magnetic field strength provided that $g\mu_B H < k_B T_{max}$.

In order to explore the interesting problem of

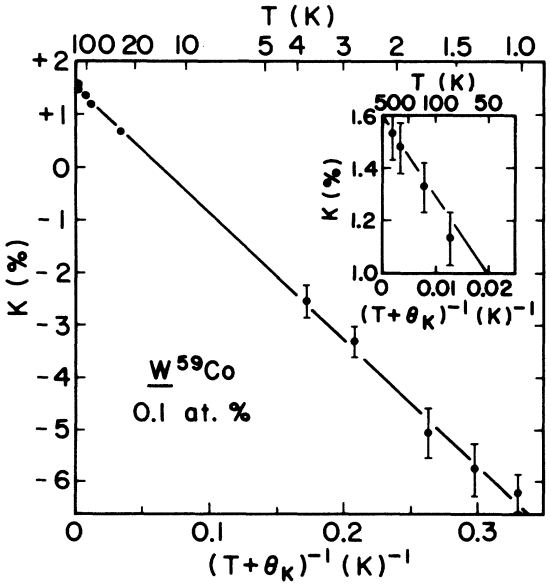

FIG. 5. Temperature dependence of ^{59}Co resonance shifts in 0.1-at.% *W*Co. The solid line corresponds to $\Theta_K = 1.8$ K.

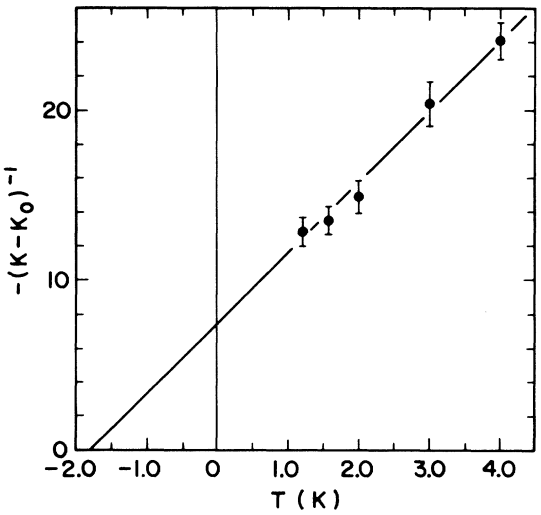

FIG. 6. Curie-Weiss plot of low-temperature ^{59}Co resonance shifts in 0.1-at.% *W*Co.

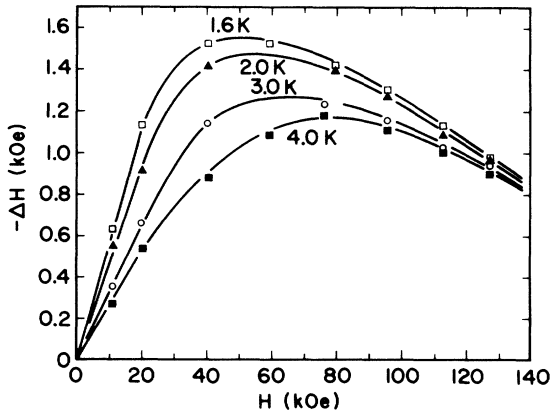

FIG. 7. Magnetic field dependence of low-temperature ^{59}Co resonance shifts in 0.1-at.% *W*Co. The solid lines are smooth fits to the data.

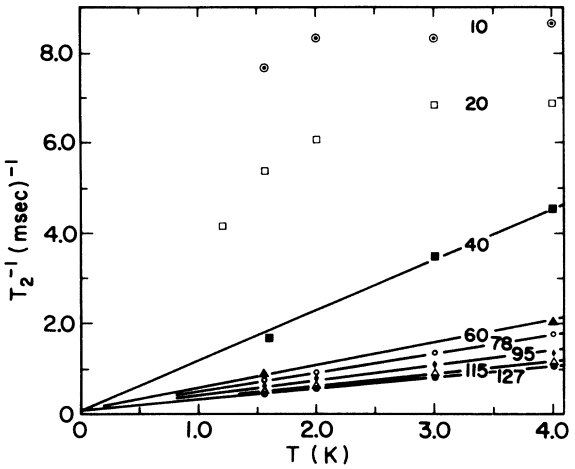

FIG. 8. Temperature dependence of the ^{59}Co nuclear relaxation rates T_2^{-1} in 0.1-at.% *W*Co for several magnetic field strengths (in kOe). The solid lines are linear fits to the high-field data.

spin dynamics in local-moment alloys, the ^{59}Co relaxation times T_2 were measured over a wide range of temperatures and field strengths. The low-temperature results are summarized in Fig. 8 for a 0.1-at.% cobalt concentration. (The lack of any significant concentration dependence was established by careful measurements on a 0.03-at.% alloy at liquid-helium temperatures in external fields of 10 and 40 kOe.) For sufficiently high field strengths the relaxation rates obey the relation $T_2^{-1} = A + BT$. The intercept $A \approx 0.1$ msec^{-1} most likely represents a cobalt nuclear spin-spin interaction rate. Information about the local-moment fluctuation spectrum is therefore contained in the term BT. Below ~40 kOe the relaxation rates follow a more complex temperature dependence, although it is reasonable to assume that a linear variation would be observed at sufficiently low temperatures.

Results of T_2 measurements at 27, 76, and 300 K are listed in Table I. The high-temperature behavior is seen to become field independent and linear in temperature, with $(T_2T)^{-1} = 100(\pm 10)$ (sec K)$^{-1}$.

TABLE I. High-temperature nuclear-spin relaxation times T_2 for 0.1 at.% ^{59}Co in *W*Co.

T(K)	H(kOe)	$T_2(\mu$sec)
26	40	137(±10)
76	40	107(±10)
300	40	35(± 5)
26	115	180(±15)
76	115	125(±10)
300	115	32(± 5)

IV. DISCUSSION

A. Crystal-field model

The experimental results presented in Sec. III confirm the close similarity between the magnetic properties of cobalt impurities in molybdenum and tungsten. Following Hirst[15] we discuss the properties of these alloys on the basis of an ionic model. The validity of this model depends critically on the impurity level width (due to covalent admixture) being smaller than the separation between the ground-state configuration $3d^n$ and the excited configurations $3d^{n\pm1}$. Such an approach appears reasonable here in view of the low Kondo temperature of *W*Co ($\Theta_K = 1.8$ K). Additional support for an ionic model is provided by the internal consistency which can be achieved in the interpretation of the NMR data.

We choose the usual $Co^{2+}(3d^7)$ configuration and assume a ^4F ground term ($L=3, S=\frac{3}{2}$). In a crystalline environment of cubic symmetry this state splits into a singlet (Γ_2) and two triplets (Γ_4, Γ_5).[16] Only the Γ_2 orbital singlet permits a negative hyperfine field as is observed in both *W*Co and *Mo*Co. For the orbital triplets the positive d-orbital hyperfine interaction always dominates the much weaker negative d-spin hyperfine interactions, and the Γ_4, Γ_5 hyperfine fields are therefore positive. We are thus led to the energy-level diagram shown in Fig. 9 which is governed by the Hamiltonian.

$$\mathcal{H}_0 = (\Delta/120)(O_4^0 + 5O_4^4) + k_\lambda \lambda \vec{L}\cdot\vec{S}. \qquad (4.1)$$

Here O_4 is the usual operator equivalent for a fourth-order crystalline potential, k_λ is an orbital reduction factor, and λ is the spin-orbit coupling constant. The spin-orbit interaction splits the

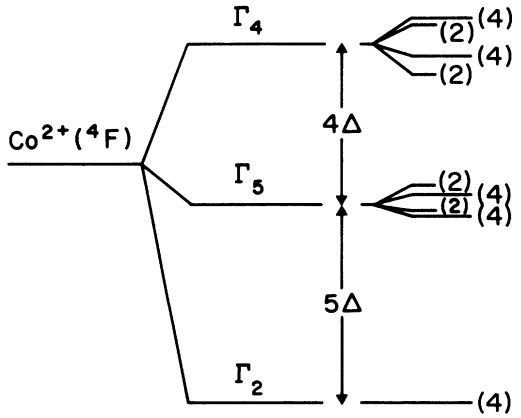

FIG. 9. Energy-level diagram for Co^{2+} (^4F) in presence of crystal-field and spin-orbit perturbations. The quantities in parentheses indicate the remaining degeneracies.

Γ_4, Γ_5 levels as indicated in Fig. 9. More importantly, it couples the Γ_2 ground state to the Γ_4, Γ_5 levels; the resulting spin-orbit induced orbital character of the ground state leads to a small positive g shift and a positive orbital contribution to the hyperfine field. The latter is presumably responsible for the small magnitude of the Γ_2 hyperfine interaction which is typically observed in the electron-spin resonance of Co^{2+} in nonmetallic crystals having four-fold or eight-fold cubic coordination.[16] We note that molybdenum and tungsten have the bcc structure (eightfold cubic symmetry). It follows that a Γ_2 ground state requires that the sign of the crystalline potential at substitutional cobalt sites correspond to a *negative* point-charge model. The opposite is the case for $3d$ impurities in the noble metals where a *positive* point-charge model accounts for the accepted ordering of the crystal-field energies.[15] Alternatively, if one assumes a $Co^+(3d^8)$ configuration [$^3F(\Gamma_2)$ ground state] or supposes that the Co^{2+} impurities occupy octahedral *interstitial* positions in molybdenum and tungsten (sixfold cubic symmetry), the crystalline potential would have the normal sign.

B. Nuclear resonance shifts

The response of the ^{59}Co nuclear spins is perturbed by the local field H_{loc} which arises primarily from hyperfine interactions with the local moment and conduction electrons. In the limit of rapid electronic relaxation [i.e., $\omega_n T_1^e \ll 1$, where ω_n is the NMR frequency and T_1^e is the electronic longitudinal spin-relaxation time], the local field may be separated into time-average and fluctuating components

$$\vec{H}_{loc}(t) = \langle \vec{H}_{loc} \rangle + \delta\vec{H}_{loc}(t) . \tag{4.2}$$

We assume that the detailed behavior of H_{loc} is determined by the following set of isotropic spin Hamiltonians.

$$\mathcal{H}_{ex} = -\mathcal{J}\vec{S}\cdot\vec{\sigma} , \tag{4.3}$$

$$\mathcal{H}_Z = g\mu_B \vec{S}\cdot\vec{H} , \tag{4.4}$$

$$\mathcal{H}_{hf} = A\vec{I}\cdot\vec{S} + A'\vec{I}\cdot\vec{\sigma} . \tag{4.5}$$

Here, $\mathcal{J}$ is an effective exchange constant resulting principally from the $l=2$ covalent admixture interaction, and σ is the conduction-electron spin. In reality, the exchange interaction is, of course, an explicit function of $\vec{k}$ and $\vec{k}'$, the wave numbers of the initial and final conduction-electron states; we have suppressed this dependence in our notation since only wave-number averages are of concern in the present case. The hyperfine coupling constants A and A' are defined in Fig. 10 and yield a resonance shift ($\Delta H \equiv \langle H_{loc}^z \rangle$)

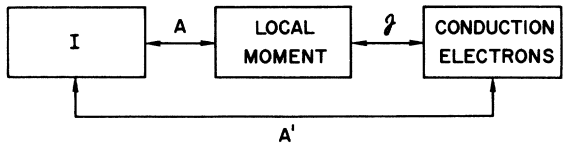

FIG. 10. Schematic representation of interacting nuclear-electronic spin system in a dilute magnetic alloy.

$$\Delta H = -(\gamma_n \hbar)^{-1}(A\langle S^z \rangle + A'\langle \sigma^z \rangle) . \tag{4.6}$$

The temperature-dependent shift $K(T)$, defined in (3.1), depends only on $\langle S^z \rangle$ which obeys a Curie law for small H/T and Θ_K/T.

$$\langle S^z \rangle = -(g\mu_B)^{-1}\chi H , \tag{4.7}$$

$$\chi = \frac{(g\mu_B)^2 S(S+1)}{3k_B(T+\Theta_K)} . \tag{4.8}$$

The g value is shifted from its free-electron value by the local-moment spin-orbit interaction as well as the conduction-electron exchange interaction (4.3). Thus $K(T)$ depends on the two unknown parameters A and g. It is convenient to define a hyperfine field $H_{hf} \equiv (g\gamma_n\hbar)^{-1}A$ and express $K(T)$ in the form

$$\Delta K/\Delta\chi = \mu_B^{-1} H_{hf} , \tag{4.9}$$

and hence

$$g^2 H_{hf} = \left[\frac{3k_B}{\mu_B S(S+1)}\right]\left[\frac{\Delta K}{\Delta(T+\Theta_K)^{-1}}\right] . \tag{4.10}$$

From our resonance-shift data we obtain

$$MoCo: g^2 H_{hf} = -47.1(\pm 1.5)\ \text{kOe}/\mu_B , \tag{4.11}$$

$$WCo: g^2 H_{hf} = -2.9(\pm 0.1)\ \text{kOe}/\mu_B . \tag{4.12}$$

In contrast to the NMR shifts, the impurity susceptibility is affected much less by any temperature-independent contributions. We may therefore combine the measured susceptibility with (4.9) to estimate H_{hf} directly. Using the published susceptibility for MoCo at $T=300$ K, $\Delta\chi = 27.5\times10^{-4}$ emu/g-atom Co,[2] we obtain $H_{hf} = -26$ kOe/μ_B and, using (4.11) or (4.8), $g=1.3$. Since the spin-orbit interaction produces a positive Co^{2+} g shift, the small g value obtained here must be attributed to the conduction-electron exchange term (4.3); it follows that $\mathcal{J}$ is negative, as expected.

The principal uncertainty in the determination of H_{hf} is associated with the unknown contribution of any "nonmagnetic" (e.g., Mo_6Co_7) second phase or strongly magnetic cobalt clusters to the reported susceptibility. This is probably not a serious problem for MoCo; in the case of WCo, however, the only available susceptibility data were

obtained for powder-metallurgical specimens which, on the basis of our NMR studies, must be assumed contamined with an appreciable fraction of W_6Co_7. As an alternative approach we use the low-temperature data, Fig. 7, to estimate the saturation hyperfine field gSH_{hf} and hence to achieve a separation of (4.12). We assume for now that the magnetic-saturation behavior of the local moment follows a Brillouin function $B_S(X)$ modified for the Kondo effect,

$$X \equiv g\mu_B H/[k_B(T+\Theta_K)], \tag{4.13}$$

and that the temperature-independent shift contribution has the high-temperature value $K_0 = 1.6\%$. Hence

$$\Delta H = -gSH_{hf} B_S(X) + K_0 H. \tag{4.14}$$

The results of fitting this expression to the 1.56- and 4.0-K shift data are displayed in Fig. 11. The fact that the agreement is not entirely satisfactory, particularly for intermediate field strengths and at the lowest temperature, is not surprising. It is now generally accepted that the destruction of the Kondo state in external fields occurs more gradually than implied by (4.13).[17] The theoretical curves plotted in Fig. 11 were obtained by forcing a fit to the initial slopes [i.e., by setting g^2H_{hf} equal to the value given in (4.12)] and to the highest-field datum at 4.0 K. This procedure gives a saturation hyperfine field for WCo, $gSH_{hf} = -3.2$ kOe, and hence $H_{hf} = -1.5$ kOe/μ_B and $g = 1.4$. It is, unfortunately, not possible to determine to what extent the assumption that $B_S(X)$ describes the actual polarization at $T = 4.0$ K and $H = 127$ kOe underestimates the saturation hyperfine field. We believe the magnitude of this error to be small. For example, a 10% increase in the saturation hyperfine field implies $g = 1.2$. This implies a larger negative g shift due to conduction-electron exchange than observed for MoCo, which seems improbable in view of the lower Kondo temperature of WCo. In this connection is is noteworthy that (4.9) and (4.12) together with the WCo susceptibility data of Booth *et al.*[1] also yield an unrealistically small g value ($H_{hf} = 2.2$ kOe/μ_B, $g = 1.1$). It is tempting to attribute this disparity to a negative conduction-electron spin polarization. Such a polarization would reduce the measured susceptibility relative to the local susceptibility. It is the latter, of course, which appears in (4.9). However, the Anderson-Clogston compensation theorem[18] is expected to apply in the present case and the net spin polarization should therefore vanish. In other words, the exchange-induced negative g shift simply reflects the *local* reduction in the impurity moment due to the admixture effect. Metallurgical problems eluded to above therefore seem to be a more credible explanation for the small g value derived from the susceptibility data.

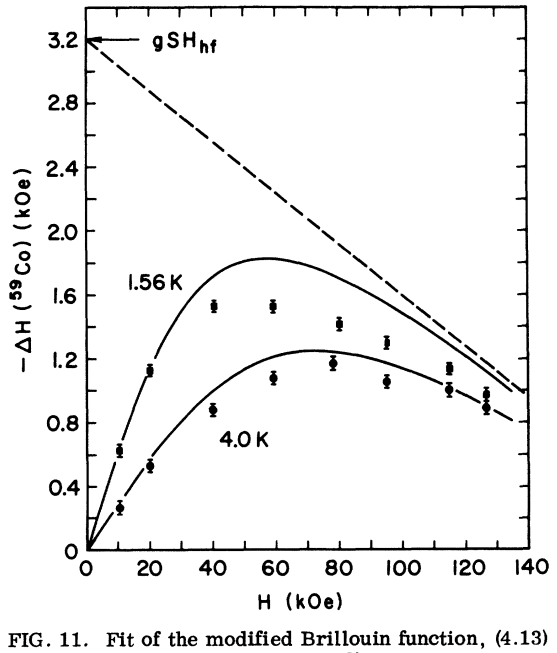

FIG. 11. Fit of the modified Brillouin function, (4.13) and (4.14), to the low-temperature ^{59}Co resonance-shift data in WCo. The dashed line indicates the assumed asymptotic behavior with slope $K_0 = +1.6\%$.

C. Nuclear-spin relaxation rates

The relaxation rate of the nuclear magnetization is determined by the fluctuating component $\delta H_{loc}(t)$ of the local field (4.2). The theory of local-moment nuclear relaxation in metals has recently been discussed in considerable detail,[19,20] and we only summarize the relevant results here. We define characteristic nuclear relaxation rates $T_{\parallel}^{-1}$ and $T_{\perp}^{-1}$ due to longitudinal and transverse local-field fluctuations, respectively, in terms of the corresponding dynamic local-moment susceptibilities.

$$T_{\parallel}^{-1} = k_B T (A/\hbar)^2 (g\mu_B)^{-2} \lim_{\omega \to 0} \mathrm{Im}\chi^{zz}(\omega)/\omega, \tag{4.15}$$

$$T_{\perp}^{-1} = k_B T (A/\hbar)^2 (g\mu_B)^{-2} \lim_{\omega \to 0} \mathrm{Im}\chi^{+-}(\omega)/2\omega, \tag{4.16}$$

which are valid for $\hbar\omega_n \ll k_B T$ and $\omega_n T_1^e \ll 1$. The susceptibilities are

$$\frac{\mathrm{Im}\chi^{zz}(\omega)}{\omega} = \chi_0^L \left(\frac{T_1^e}{1+(\omega T_1^e)^2} \right), \tag{4.17}$$

$$\frac{\mathrm{Im}\chi^{+-}(\omega)}{2\omega} = \chi_0^T \left(\frac{T_2^e}{1+[(\omega-\omega_e)T_2^e]^2} \right), \tag{4.18}$$

where $\chi_0^L = g\mu_B \partial\langle S^z\rangle/\partial H$ and $\chi_0^T = g\mu_B \langle S^z\rangle/H$. The

longitudinal and transverse electronic relaxation rates are given to lowest order in $\mathcal{J}\rho$ (where ρ is the conduction-electron density of states at the Fermi level for one spin direction) by

$$\frac{1}{T_1^e} = \frac{\pi(g\mu_B)^2(\mathcal{J}\rho)^2\langle S^z\rangle x}{4\hbar \sinh^2(x/2)\chi_0^L}\,, \tag{4.19}$$

$$\frac{1}{T_2^e} = \frac{\pi(g\mu_B)^2(\mathcal{J}\rho)^2}{2\hbar\chi_0^T}\left\{S(S+1) - \langle S^z\rangle \coth\left(\frac{x}{2}\right) + \frac{(y-x)}{2y}\langle S^z\rangle\left[\coth\left(\frac{y-x}{2}\right) + \coth\left(\frac{x}{2}\right)\right]\right\}, \tag{4.20}$$

where $x \equiv \hbar\omega_e/k_BT$ and $y \equiv \hbar\omega/k_BT$. The local-moment frequency $\omega_e = g\mu_BH/\hbar$ must be corrected for any conduction-electron induced shifts by proper choice of g value. We also emphasize that (4.19) and (4.20) are only valid at sufficiently high temperatures and/or magnetic field strengths where Kondo anomalies in the local-moment fluctuation spectrum are unimportant.

Two limiting regimes may be distinguished. At low temperatures ($\omega_e T_2^e \gg 1$) the fluctuations are anisotropic, with

$$T_\parallel^{-1} \approx A^2 e^{-x}/\pi\hbar\omega_e S(\mathcal{J}\rho)^2\,, \tag{4.21}$$

for $x > 1$, and

$$T_\perp^{-1} \approx \pi k_B T A^2 S^2(\mathcal{J}\rho)^2/2\hbar^3\omega_e^2\,. \tag{4.22}$$

At high temperatures ($\omega_e T_2^e \ll 1$) the fluctuations are isotropic, with

$$T_\parallel^{-1} = T_\perp^{-1} \approx A^2 S(S+1)/3\hbar\pi k_B T(\mathcal{J}\rho)^2\,. \tag{4.23}$$

The transverse nuclear relaxation time T_2 measured in our experiments can usually be written as

$$T_2^{-1} = T_\parallel^{-1} + T_\perp^{-1}\,, \tag{4.24}$$

provided that the hyperfine interaction is isotropic. However, for the case in which only the $+\frac{1}{2} \longleftrightarrow -\frac{1}{2}$ transition is observed, the contribution of the transverse fluctuations is enhanced. Adapting the calculation of Walstedt[21] to the present case, we find for the central transition

$$T_2^{-1} = T_\parallel^{-1} + \tfrac{1}{2}[4I(I+1) - 1]\,T_\perp^{-1}\,. \tag{4.25}$$

For ^{59}Co ($I = \frac{7}{2}$) this expression leads to a transverse enhancement factor of 31. As a consequence, $T_2^{-1} \propto T_\perp^{-1}$ over almost the entire range of our measurements.

An inspection of (4.22) and (4.23) indicates that the ^{59}Co relaxation rate T_2^{-1} should vary as T/H^2 at low temperatures (for large H/T) and as $1/T$ (independent of H) at high temperatures. Although the low-temperature behavior of T_2 in WCo is at least qualitatively as expected, the high-temperature behavior is not. According to Table I the high-temperature rates, although independent of H, appear to *increase* linearly with temperature rather than decrease. This observation can be readily explained by the direct Korringa relaxation to the conduction-electron spins. This process yields a relaxation rate for the $+\frac{1}{2} \longleftrightarrow -\frac{1}{2}$ transition

$$T_2^{-1}(\text{Korr.}) = (I+\tfrac{1}{2})^2(2l+1)(\pi/\hbar)k_BT(A'\rho')^2\,, \tag{4.26}$$

where l specifies the dominant partial wave in the relaxation process. The density of itinerant d electrons at the cobalt sites is likely to be small and the principal direct coupling to the conduction electrons is therefore the s-contact interaction. The density of states ρ' in (4.26) is then the effective s density and A' the s-contact hyperfine constant $[A'(g\gamma_n\hbar)^{-1} \approx 10^6\ \text{Oe}/\mu_B]$. Since $A'/A \sim 10^3$ in WCo, it is obvious that T_2^{-1}(Korr.) will become dominant at moderately high temperatures. We may write

$$T_2^{-1} = T_2^{-1}(\text{loc}) + T_2^{-1}(\text{Korr.})\,, \tag{4.27}$$

where the local-moment contribution T_2^{-1}(loc) is to be identified with (4.25). In addition, one must consider the possibility of interference between the two relaxation processes. In the low-temperature regime ($\omega_e T_2^e > 1$) one obtains the cross term[19,20]

$$T_\perp^{-1}(\text{cross}) = \pi k_B T A A' \mathcal{J}\rho^2\langle S^z\rangle(\hbar\omega_e)^{-1}\,. \tag{4.28}$$

The interference is seen to be either constructive or destructive depending on the sign of $AA'\mathcal{J}$. It is important to note that $T_\perp^{-1}$(cross) vanishes unless the conduction-electron partial-wave characters responsible for A' and $\mathcal{J}$ are identical. In the present case we expect $\mathcal{J}$ to involve the $l = 2$ component while A' most likely involves the $l = 0$ component. For this reason we neglect the cross term in the analysis of our relaxation data. Finally, we mention for completeness that conduction-electron correlation effects have been ignored throughout. This should be a reasonable approximation for MoCo and WCo since the exchange enhancements of the respective host susceptibilities

are believed to be small.

The theoretical predictions for the local-moment process, (4.15)–(4.20), may be compared with the *W*Co relaxation data by letting $[T_2(\text{Korr.})T]^{-1} = 100$ (sec K)$^{-1}$ in accordance with the measured high-temperature rates and treating $\mathcal{J}\rho$ as an adjustable parameter. By choosing $|\mathcal{J}\rho| = 0.40$, reasonable agreement with observations was obtained for the highest field strength. It is here that $T_2^{-1}(\text{loc})$ is expected to be least sensitive to the assumptions inherent in the local-moment fluctuation theory. The other parameters $[g = 1.4, S = \frac{3}{2}, -(g\gamma_n\hbar)^{-1}A = 1.5 \text{ kOe}/\mu_B]$ were taken from the resonance-shift analysis discussed above.

The result of calculating T_2^{-1} according to (4.25)–(4.27) are shown in Fig. 12 together with the experimental data. Although the over-all agreement is encouraging, significant differences between theory and experiment appear at low temperatures. This disparity increases with decreasing field strength. It is clear that the predicted H^{-2} divergence of the relaxation rate does not occur. Instead, our results suggest that the relaxation rates are tending towards a limiting value. Two obvious explanations may be advanced for this behavior. In the first place, because of the finite impurity concentration, impurity-impurity exchange interactions will result in a local-moment fluctuation spectrum which becomes independent of magnetic-field strength and temperature. This occurs below a temperature $\omega_E/[(\mathcal{J}\rho)^2 k_B]$, where ω_E is an effective exchange frequency. Thus, for $\omega_e < \omega_E$ the nuclear relaxation rates are expected to be independent of both field strength and temperature. Whether the latter applies to our alloys can not be determined from the available data. In any event, because of the absence of any concentration dependence we can reject impurity interactions as a plausible explanation for the disparity between experiment and theory.

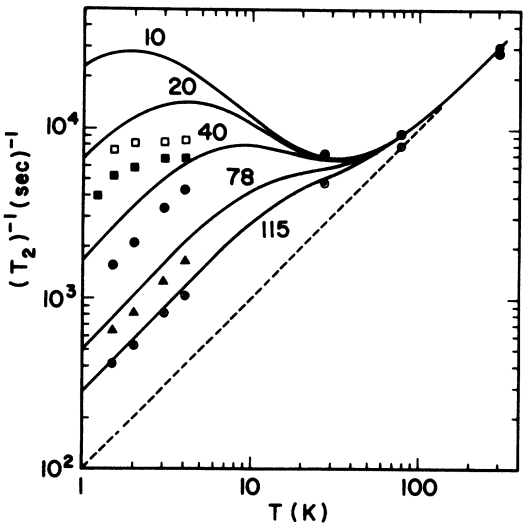

FIG. 12. Comparison of experimental and theoretical ^{59}Co relaxation rates in *W*Co for several field strengths (in kOe) as discussed in the text. The experimental data have been adjusted by subtracting the temperature-independent term (0.1 msec^{-1}). The dashed line gives the Korringa rate $100T$ sec^{-1}.

We propose, instead, that the observed field dependence of the low-temperature relaxation rates is a direct consequence of Kondo anomalies in the local-moment spectral-density function. While no rigorous theory exists for the low-temperature dynamic behavior of Kondo alloys it is generally accepted that the local-moment relaxation rates are enhanced significantly over the predictions (4.19) and (4.20) of lowest-order perturbation theory.[17] It is reasonable to assume that the fluctuations become isotropic for sufficiently low temperature and weak magnetic fields, and that this spectral density extends to a frequency of order $k_B\Theta_K/\hbar$. Since the static susceptibility $\text{Re}\chi(0)$ is proportional to $(k_B\Theta_K)^{-1}$ in the low-temperature limit, one may infer from the Kramers-Kronig relation that

$$\lim_{\omega\to 0} \frac{\text{Im}\chi(\omega)}{\omega} \propto (k_B\Theta_K)^{-2}, \tag{4.29}$$

independent of both H and T. This leads to a scaling relationship $T_\parallel^{-1} = T_\perp^{-1} \propto H_{\text{hf}}^2 T/\Theta_K^2$ for $T < \Theta_K$, which should provide a basis of comparison for different alloys having identical impurity spin S. Support for this relationship can be found in the experimental relaxation rates for[7] *Mo* ^{59}Co and[8] *Au* ^{51}V (for both alloys the ionic model suggests $S = \frac{3}{2}$). As shown in Table II, the product $(\gamma_n^2 T_1 T)^{-1}(\Theta_K/H_{\text{hf}})^2$ have similar magnitudes. Assuming this quantity to have the same magnitude for *W* ^{59}Co as for *Mo* ^{59}Co yields a prediction for the limiting low-temperature, low-field ^{59}Co relaxation rate in the tungsten alloy of $(T_2T)^{-1} = 12$ (msec K)$^{-1}$, which is only slightly greater than the experimental value near 1 K and 10 kOe. This result gives additional confidence that the disparity between perturbation theory and experiment is a direct manifestation of the Kondo effect.

There remains the question whether the nuclear-resonance properties of a transition-element impurity in a metallic host can distinguish between nonmagnetic and magnetic regimes. It is well-known that the former is characterized by isotropic localized spin and orbital fluctuations of the form $\text{Im}\chi_i(\omega) \propto (\tau_i^{-1} - i\omega)^{-1}$. Spin-orbit effects are assumed to be unimportant in this limit and

TABLE II. Comparison of impurity nuclear spin-lattice relaxation rates in AuV and MoCo.

	$(\gamma_n^2 T_1 T)^{-1}$ (10^{-6} sec K^{-1} Oe^2)	Θ_K (K)	H_{hf} (kOe/μ_B)	$(\gamma_n^2 T_1 T)^{-1}(\Theta_K/H_{hf})^2$ (10^{-9} sec K)
Au ^{51}V	1.2(±0.2)	290	−45	19
Mo ^{59}Co	10(±1)	45	−26	33

the two fluctuation modes are consequently independent. In the Hartree-Fock approximation one finds simple Korringa-type relations which, in the absence of crystal-field splittings, are given by[22,23]

$$K^2_{\text{spin}}(T_{1,\text{spin}}T) = 5\mathcal{S}\ , \tag{4.30}$$

$$K^2_{\text{orb}}(T_{1,\text{orb}}T) = 10\mathcal{S}\ , \tag{4.31}$$

where $\mathcal{S} = \hbar(\gamma_e/\gamma_n)^2\ (4\pi k_B)^{-1}$. Actually, Shiba[24] has shown that these results apply to any order of the Coulomb interaction on the impurity site for the fivefold degenerate Anderson model provided $T < \Theta_K$ and $g\mu_B H < k_B\Theta_K$. In the earlier work on AuV and MoCo the expressions (4.30) and (4.31) were used to separate the spin and orbital contributions to K and T_1T. The orbital shifts obtained in this way were in good agreement with the high-temperature intercepts of the experimental K vs $(T+\Theta_K)^{-1}$ plots. This interpretation requires that the spin susceptibility is temperature dependent while the orbital susceptibility is independent of temperature in the range of the experiments. The fact that $\tau^{-1}_{\text{spin}} < \tau^{-1}_{\text{orb}}$ can be used to rationalize such behavior. Actually, the interpretation of the AuV and MoCo data was not strongly dependent on the orbital Korringa relation (4.31) because the spin interaction is dominant in these alloys as evidenced by the negative resonance shifts. Essentially identical results would be obtained if we assume $T^{-1}_{1,\text{orb}} = 0$ and let $T_1^{-1} = T^{-1}_{1,\text{spin}}$ [i.e., we assume that only (4.30) applies as the magnetic limit is approached by an S-state impurity]. In this connection we note that the theory has been less successful in the case of the nonmagnetic alloy AuCo for[25] which the S-state limit probably does not apply. Here the shift is large and *positive* (i.e., the orbital interaction is presumed to be dominant); the relaxation rate, on the other hand, is anomalously slow suggesting that the orbital hyperfine interaction in AuCo is ineffective as a nuclear spin relaxation mechanism.

Recently, Alloul[26] has shown that the low-temperature (1–4K) resonance shifts and relaxation rates of ^{63}Cu nuclei near iron impurities in the "classic" Kondo system CuFe ($\Theta_K = 27.6$ K) also obey the prediction (4.30). Unfortunately, the copper hyperfine coupling is presumably insensitive to any orbital fluctuations of the impurity, and the ^{63}CuFe experiments are, therefore, unable to verify the existence of independent spin- and orbital-fluctuation modes predicted by the Anderson model. Such independence does not exist, of course, in the ionic model employed in the present paper; instead, the spin and orbital degrees of freedom are tightly coupled by intra-atomic correlation (Hund's rule) effects and the spin-orbit interaction. Any temperature-independent resonance shift is due to field-induced admixtures of excited states into the zero-field ground state; there is no strong nuclear relaxation mechanism associated with this process because of the absence of low-frequency fluctuations. The impurity is therefore characterized by a single fluctuation mode.

The scaling relationship discussed above implies that this mode also leads to a Korringa relation which, however, depends explicitly on the impurity spin. In order to display this result more clearly we carry out the Kramers-Kronig inversion using (4.8) and assuming a constant spectral density $\text{Im}\chi(\omega)/\omega$ with a sharp cutoff at $\omega = \pm k_B\Theta_K/\hbar$. We obtain in the low-temperature limit

$$K^2T_1T = \frac{8S(S+1)}{3}\left(\frac{g\mu_B}{\gamma_n\hbar}\right)^2\left(\frac{\hbar}{4\pi k_B}\right) \tag{4.32}$$

where $T_1^{-1} = 2T_\perp^{-1}$, which is seen to be independent of Θ_K. The expression differs from (4.30) in its dependence on S and the fact that the actual impurity g value is indicated rather than the free-electron g value assumed in the derivation of (4.30). For $S = 1$ the two expressions are essentially identical; this striking similarity must be regarded with some suspicion, however, since the functional form of $\text{Im}\chi(\omega)/\omega$ assumed here has no rigorous theoretical basis.

The Korringa rate $[T_2(\text{Korr.})T]^{-1} = 100$ (sec K)$^{-1}$ inferred from the high-temperature data can be used to estimate the s-contact resonance shift (K_s) at the impurity site in WCo. Combining (4.26) with the usual expression

$$K_s = (\gamma_n\hbar)^{-1}\mu_B A'\rho' \tag{4.33}$$

yields a shift $K_s = 0.54\%$ which is presumably posi-

tive. It is interesting to note that this shift is approximately twice as large as the Knight shift in pure copper metal.[27] Because of the neglect of possible exchange-enhancement effects, our estimate of K_s represents a lower limit.[28] This is not a significant problem, however, since collective-electron effects are likely to be unimportant in tungsten. The large magnitude of K_s must be attributed to a larger s-like density of states at the Fermi energy for Co in W than is observed for the noble metals. This is not surprising in view of the large screening charge required by the divalent cobalt ion. Finally, assuming that the observed high-temperature shift in W^{59}Co is the sum of s-contact conduction-electron and d-orbital (Van Vleck) local-moment contributions

$$K_0 = K_s + K_{VV} \tag{4.34}$$

we obtain $K_{VV} = +1.1\%$.

D. Spin and orbital parameters

The preceding analysis has yielded cobalt g and H_{hf} values for *Mo*Co and *W*Co. We now wish to examine the consequences of the ionic crystal-field model by separating these quantities into spin and orbital contributions as a function of the parameter Δ. It is also of interest to compare the exchange constant inferred from the *W*Co relaxation data with that implied by the negative g shift. Because of the great simplifications inherent in our model we shall not attempt to account for the relatively small differences between *Mo*Co and *W*Co; instead, our discussion will be limited to a consideration of the *W*Co data.

We adopt the following procedure: (i) For a given crystal-field splitting Δ we diagonalize $\mathcal{H}_0$, as defined by (4.1), using straightforward numerical techniques. (ii) We introduce the Zeeman perturbation

$$\mathcal{H}_Z = \mu_B \vec{H} \cdot (k_Z \vec{L} + 2\vec{S}) , \tag{4.35}$$

where k_Z is the orbital reduction factor appropriate to the Zeeman interaction, and compute the appropriate matrix elements of L and S in the representation which diagonalizes $\mathcal{H}_0$. We have also assumed for computational convenience that H is oriented along [100]; the cubic anisotropy[29] is expected to be small in the present case because our results require a small value of $k_\lambda \lambda/\Delta$, although the actual magnitude of this quantity cannot be determined from our data alone. The Γ_4, Γ_5 ground-state admixtures are therefore small and any anisotropy can be safely neglected. The spin and orbital g values are

$$g_S = -\tfrac{4}{3}\langle 0|S^z|0\rangle , \tag{4.36}$$

$$g_L = -\tfrac{2}{3}k_Z\langle 0|L^z|0\rangle , \tag{4.37}$$

where $|0\rangle \equiv |\Gamma_2, m_S = -S\rangle$. The measured g value is then given by

$$g = \eta(g_S + g_L) . \tag{4.38}$$

The parameter η describes the g shift resulting from the conduction-electron exchange (4.3). In effect, we assume that the field experienced by the local moment is the sum of the external field H and a molecular field $(\eta - 1)H$ due to the conduction-electron exchange term. The assumption that the exchange coupling affects the spin and orbital degrees of freedom equally can, in principle, not be justified; we introduce this simplification only because the relatively small g_L values make more complex parameterizations meaningless. (iii) We decompose the hyperfined field H_{hf} into its spin and orbital components by utilizing the experimentally determined saturation hyperfine field

$$gSH_{hf} = \eta S(g_S H_{hf}^{(spin)} + g_L H_{hf}^{(orb)}) , \tag{4.39}$$

and Van Vleck resonance shift

$$K_{VV} = \mu_B \eta^2 \sum_{i \neq 0} (2\langle i|S^z|0\rangle + k_Z\langle i|L^z|0\rangle)[E(i) - E(0)]^{-1}(4H_{hf}^{(spin)}\langle 0|S^z|i\rangle + 2k_Z H_{hf}^{(orb)}\langle 0|L^z|i\rangle) , \tag{4.40}$$

where the sum extends over the Γ_4, Γ_5 manifolds. The term depending on $H_{hf}^{(spin)}$ in (4.40) is small provided $k_\lambda \lambda/\Delta < 1$ and can usually be neglected.

Choosing the free-ion value[16] $\lambda = -176$ cm^{-1}, and letting $k_Z = k_\lambda = 1$ yields the spin and orbital g values shown in Fig. 13; the corresponding exchange parameters η were derived from (4.38) using $g = 1.4$. Carrying out the perturbation calculation for $K_{VV} = 0.011$ according to (4.40) and solving (4.39) and (4.40) for $H_{hf}^{(spin)}$ and $H_{hf}^{(orb)}$ leads to the results shown in Fig. 14. Because of the many uncertainties, particularly in k_Z and k_λ, the absolute magnitudes should be viewed with some caution. The indicated trends and, more generally, the dependence of the calculated quantities on the various parameters can be understood by means of the following scaling relations which become exact in the limit $k_\lambda \lambda/\Delta \to 0$:

$$\text{(a)}\ g_S \approx 2 , \tag{4.41}$$

$$\text{(b)}\ g_L \propto k_Z k_\lambda \lambda/\Delta , \tag{4.42}$$

(c) $\eta = g(g_S + g_L)^{-1} \approx g/2$, (4.43)

(d) $H_{hf}^{(orb)} \propto K_{VV}/\chi_{VV} \propto K_{VV}\eta^{-2}k_z^{-2}\Delta$. (4.44)

The small magnitude of H_{hf} implies $H_{hf}^{(spin)} g_S \approx -H_{hf}^{(orb)} g_L$; thus,

(e) $H_{hf}^{(spin)} \approx -H_{hf}^{(orb)} g_L/g_S \propto -K_{VV} k_\lambda \lambda \eta^{-2} k_z^{-1}$. (4.45)

Although it is not possible to determine Δ, we note that the free-atom value of $H_{hf}^{(orb)}$ is approximately 600 kOe.[30] For reasonable values of k_z, Δ therefore lies near 1000 cm^{-1}.

Because η is relatively insensitive to the model parameters it is possible to determine $\mathcal{J}\rho$ from the observed g value, using[31]

$\eta = [1 + \frac{1}{2}(g_\sigma/g)\mathcal{J}\rho]$, (4.46)

where $g_\sigma \approx 2$ is the conduction-electron g value.

Choosing $\eta = 0.60$, we obtain $\mathcal{J}\rho = -0.56$. This is close to the value $|\mathcal{J}\rho| = 0.4$ inferred from the relaxation data. Although the close agreement is gratifying, it has only qualitative significance because of several complicating (and unknown) factors, ignored in our analysis, which affect the static and dynamic local-moment properties differently. Among these are the wave-number dependence of $\mathcal{J}$, intrinsic differences in the way covalent admixture contributes to the g shift and local-moment relaxation rates,[31] and the fact that the exchange coupling for $l > 0$ involves multiple orbital scattering channels.

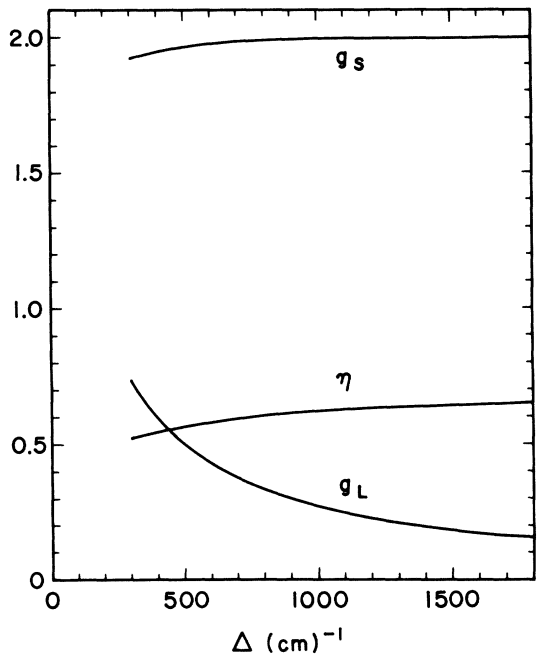

FIG. 13. Variation of calculated spin and orbital g values and g shift with crystal-field splitting parameter according to the ionic model.

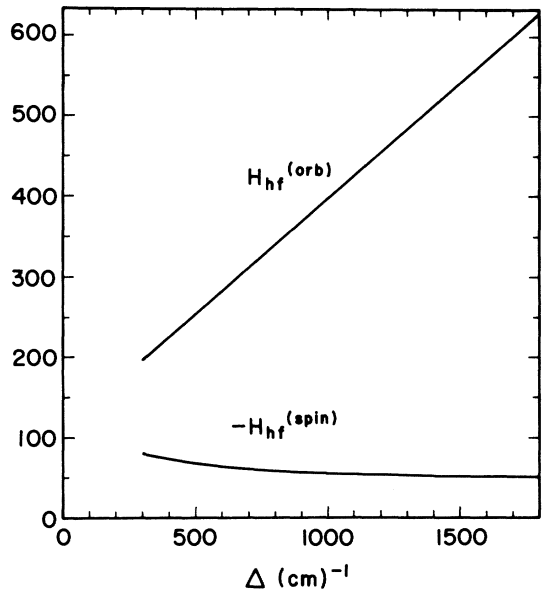

FIG. 14. Variation of calculated spin and orbital hyperfine fields (in kOe/μ_B) with crystal-field splitting parameter according to the ionic model.

V SUMMARY

The present study has provided detailed information about the magnetism of dilute cobalt impurities in molybdenum and tungsten. A summary of the principal quantities for the two alloys derived from our measurements is given in Table III. An ionic model based on a Γ_2 orbital-singlet ground state arising from the Co^{2+} $3d^7(^4F)$ term perturbed by spin-orbit, crystal-field, and local-moment/conduction-electron exchange interactions can account satisfactorily for the observed static as well as dynamic properties. The sign of the crystalline potential at the purity appears to be anomalous if it is assumed that the cobalt atoms occupy substitutional sites in the bcc host lattice. The lowest excited state (Γ_5) lies approximately 5000 cm^{-1} above the ground state.

We believe that the small cobalt hyperfine fields result from a near cancellation of the negative d-

TABLE III. Summary of parameter values derived from ^{59}Co NMR data.

	Θ_K (K)	g	H_{hf} (kOe/μ_B)	K_0(%)
*Mo*Co	45(±3)	1.3	−26	+1.8(±0.1)
*W*Co	1.8(±0.2)	1.4	−1.5	+1.6(±0.1)

spin hyperfine field of the Γ_2 ground state by a positive spin-orbit induced orbital hyperfine field. Similarly the positive temperature-independent contributions to the resonance shifts result from field-induced orbital admixture effects. The large negative g shifts inferred from the resonance shift data give evidence for strong negative local-moment–conduction-electron exchange interactions in both *Mo*Co and *W*Co. The magnitude of this interaction is consistent with the observed low-temperature ^{59}Co relaxation rates in *W*Co. Simple scaling relations link these results with impurity relaxation rates in other Kondo alloys such as *Mo*Co and *Au*V. Despite significant fundamental differences between the Anderson (Hartree-Fock) and ionic models it appears that the impurity nuclear-spin relaxation rates cannot distinguish clearly between the nonmagnetic and magnetic approaches to the magnetic impurity problem when $T \ll \Theta_K$. Whether this is a fortuitous circumstance or indicates a fundamental relationship between the properties of localized-spin-fluctuation and Kondo systems remains uncertain.

ACKNOWLEDGMENTS

The author is greatly indebted to D. C. Barham for carrying out the NMR experiments reported here and for his contributions to the solution of the materials problems. The support of R. C. Knauer in performing the Mössbauer experiment is also acknowledged.

---

*This work was supported by the U.S. Energy Research and Development Administration (ERDA).

[1]J. G. Booth, K. C. Brog, and W. H. Jones, Jr., Proc. Phys. Soc. Lond. 92, 1083 (1967).
[2]H. Claus, Phys. Rev. B 5, 1134 (1972).
[3]N. V. Volkenshtein, L. A. Ugodnikova, and Yu. N. Tsiovkin, Sov. Phys.-Solid State 12, 1160 (1970).
[4]K. C. Brog, W. H. Jones, Jr., and G. S. Knapp, Solid State Commun. 5, 913 (1967); K. C. Brog (unpublished).
[5]T. Sugawara, M. Takano, and S. Takayanagi, J. Phys. Soc. Jpn. 36, 451 (1974).
[6]K. C. Brog, W. H. Jones, Jr., and J. G. Booth, J. Appl. Phys. 38, 1151 (1967).
[7]A. Narath, K. C. Brog, and W. H. Jones, Jr., Phys. Rev. B 2, 2618 (1970).
[8]A. Narath and A. C. Gossard, Phys. Rev. 183, 391 (1969).
[9]A. Narath, Solid State Commun. 10, 521 (1972).
[10]K. Kume, J. Phys. Soc. Jpn. 23, 1226 (1967).
[11]T. J. Quinn and W. Hume-Rothery, J. Less-Common Met. 5, 314 (1963).
[12]M. Hansen, *Constitution of Binary Alloys*, 2nd ed. (McGraw-Hill, New York, 1958), p. 518.
[13]A. Narath and D. C. Barham, Rev. Sci. Instrum. 45, 100 (1974).
[14]R. E. Walstedt, J. H. Wernick, and V. Jaccarino, Phys. Rev. 162, 301 (1967).
[15]L. L. Hirst, Arch. Sci. Genev. 27, 2 (1974).
[16]A. Abragam and B. Bleaney, *Electron Paramagnetic Resonance of Transition Ions* (Clarendon, Oxford 1970).
[17]W. Götze, Arch. Sci. Genev. 27, 357 (1974).
[18]P. W. Anderson and A. M. Clogston, Bull. Am. Phys. Soc. 2, 124 (1961).
[19]R. E. Walstedt and A. Narath, Phys. Rev. B 6, 4118 (1972).
[20]A. Narath, Phys. Scr. 11, 237 (1975); Erratum (to be published).
[21]R. E. Walstedt, Phys. Rev. Lett. 19, 146 (1967); 19, 816 (1967).
[22]B. Caroli, P. Lederer, and D. Saint-James, Phys. Rev. Lett. 23, 700 (1969).
[23]L. Dworin and A. Narath, Phys. Rev. Lett. 25, 1287 (1970).
[24]H. Shiba, Prog. Theor. Phys. 54, 967 (1975).
[25]A. Narath and D. C. Barham, Phys. Rev. B 7, 2195 (1973).
[26]H. Alloul, Phys. Rev. Lett. 35, 460 (1975).
[27]D. R. Teeters, thesis (University of California, Berkeley, 1955) (unpublished).
[28]A. Narath and H. T. Weaver, Phys. Rev. 175, 373 (1968).
[29]F. S. Ham, G. W. Ludwig, G. D. Watkins, and H. H. Woodbury, Phys. Rev. Lett. 5, 468 (1960).
[30]A. J. Freeman and R. E. Watson, in *Magnetism*, Vol. IIA, edited by G. T. Rado and H. Suhl (Academic, New York, 1965), p. 290.
[31]J. Zitkova-Wilcox, Arch. Sci. Genev. 27, 141 (1974).